

Computer image analysis of brain CT images for discriminating hypodense cerebral lesions in children

D. CAVOURAS* and P. PRASSOPOULOS†

Department of Medical Instruments,
School of Technological Applications,
Technological Educational Institute of Athens, Greece
†Department of Diagnostic Radiology, University Hospital,
Medical School of Crete, Greece

(Received August 1993)

Abstract. A computer software system was designed for the automatic discrimination of focal oedemas from local glioses in brain CT examinations. Image analysis methods were applied to the images of 77 CT examinations of children with focal oedemas (42) or local glioses (35). Textural features derived from the co-occurrence matrix of the lesion's image and a neural network classifier (the multilayer perceptron) were employed for the design of the system. Best classification accuracy (89.6%) was achieved by two textural features (contrast-difference entropy), one hidden layer and three hidden nodes of the classifier. The proposed software system provides new textural information and may be of value to the radiologist in differentiating focal oedemas from local glioses, especially in small lesions, where other radiological criteria are not evident.

Keywords: Image, computer analysis; Brain, focal lesion; Computed tomography, children; Neural network, classification.

1. Introduction

Focal oedema and local gliosis are the most frequent hypodense cerebral lesions in brain CT examinations of children. In assessing the lesion's nature [1, 2], the radiologist evaluates the clinical history of the patient and the specific characteristics of the CT images. CT findings usually concern the regularity and sharpness of the lesion's margin and the effect on neighbouring brain parenchyma. However, pictorial information related to the internal structure of the lesion is of poor diagnostic value, since in most cases both focal oedemas and local glioses appear homogeneous and have similar attenuation values.

Here, brain CT images of children with focal oedema or local gliosis were processed employing image analysis methods. Only small lesions were considered, since they are not easily differentiated by visual inspection. The aim was to analyse the internal structure of the lesion in order to obtain information concerning its nature. This textural information, together with a neural network classifier, was used in the design of a software system for the automatic discrimination between focal oedemas and local glioses.

*Address for correspondence: Professor D. Cavouras, Department of Medical Instruments, Technological Educational Institute of Athens, 37-39 Esperidon Street, Kallithea 17671, Athens, Greece.

2. Material and methods

The study comprised 77 non-contrast-enhanced CT examinations of children 3–12 years old (51 boys, 26 girls) with focal oedema (42) or local gliosis (35) < 2 cm in maximum cross-sectional diameter. Diagnosis was confirmed on the basis of the patient's history, clinical data, and CT follow-up examinations. All examinations were performed on a Philips LX CT scanner, with 320×320 reconstruction matrix, 10 mm slice thickness, 120 kV, 150 mA, and 2.9 s scan time. No additional CT sections were obtained for the purposes of this work.

In each examination the CT section through the maximum cross-sectional diameter of the brain damage was selected; the CT density matrix of the lesion's central region (figure 1)— 10×10 or 20×20 pixels depending on the size of the damage—was transferred to a computer (AT, 486/33 Mhz) for further processing.

2.1. Feature generation

From each CT density matrix 16 textural features were calculated. Four were extracted from the lesion's density histogram, which gives the frequency of density values in the lesion's image matrix: mean value, variance, skewness and kurtosis. The rest were computed from the co-occurrence matrix [3, 4], which is a two-dimensional histogram describing the frequency with which two adjacent CT density values occur in the lesion's image matrix. The co-occurrence matrix was calculated as the mean of the values of the 0, 45, 90 and 135° co-occurrence matrices [3], with step length of one pixel; the 12 co-occurrence features were computed as described by Haralick *et al.* [3].

2.2. Feature reduction

The discriminatory ability of each of the 16 textural features was tested employing Student's *t*-test. Only the best discriminating features ($p < 0.001$) were selected, and were further employed in the design of the computer software for discriminating oedemas from glioses (SDEG).

2.3. Classification

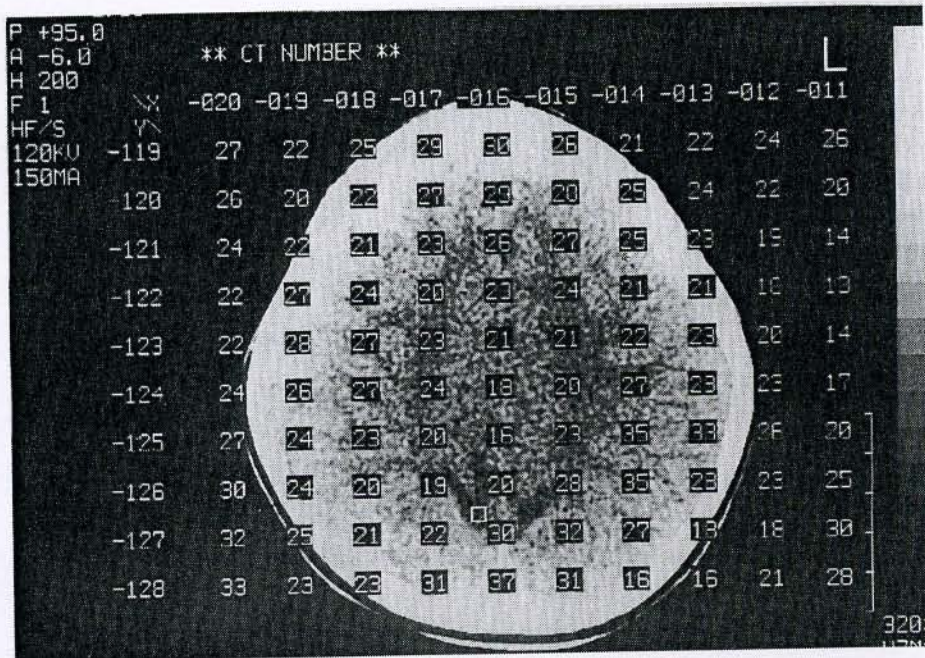
Classification was performed by means of the multilayer perceptron (MLP) classifier [5, 6] (neural network). In each node of a hidden layer or output layer of the MLP classifier (figure 2), the output $y(j)$ of node j is related to its inputs by relation (1):

$$y(j) = \frac{1}{1 + \exp(-S(j))}, \quad (1)$$

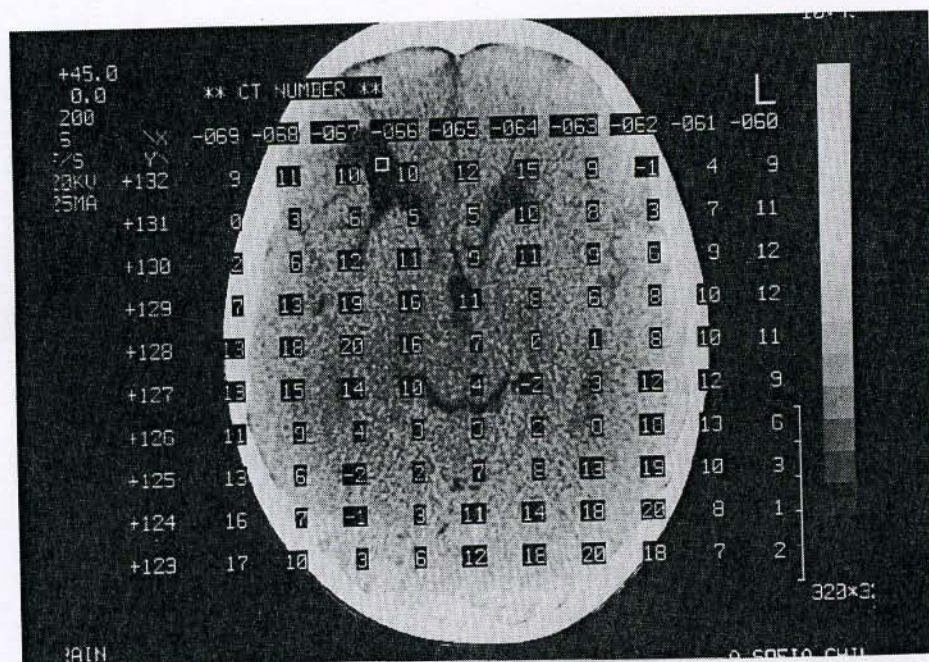
where

$$S(j) = \sum_{i=1}^N y(i)w(i,j) \quad (2)$$

and $w(i,j)$ = connection weight between previous node i and current node j ; $y(i)w(i,j)$ = weighted output of previous node i , which is used as input to node j ; N = number of inputs to node j ; and $S(j)$ = sum of all weighed inputs $y(i)w(i,j)$ of the previous layer to node j . The connection weights $w(i,j)$ between different layer



(a)



(b)

Figure 1. Brain CT images of children with superimposed density matrix of (a) local gliosis and (b) focal oedema.

nodes of the MLP classifier are calculated iteratively until they stabilize, by the following equation:

$$w(i,j)^{n+1} = w(i,j)^n + ad(j)y(i) + z(w(i,j)^n - w(i,j)^{n-1}), \quad (3)$$

where $(n+1)$, n , $(n-1)$ = next, present, previous; a , z = constants; $d(j)$ = error between the desired $t(j)$ and actual $y(j)$; and output of node j , which for an output layer node is given by equation (4)

$$d(j) = (t(j) - y(j))y(j)(1 - y(j)), \quad (4)$$

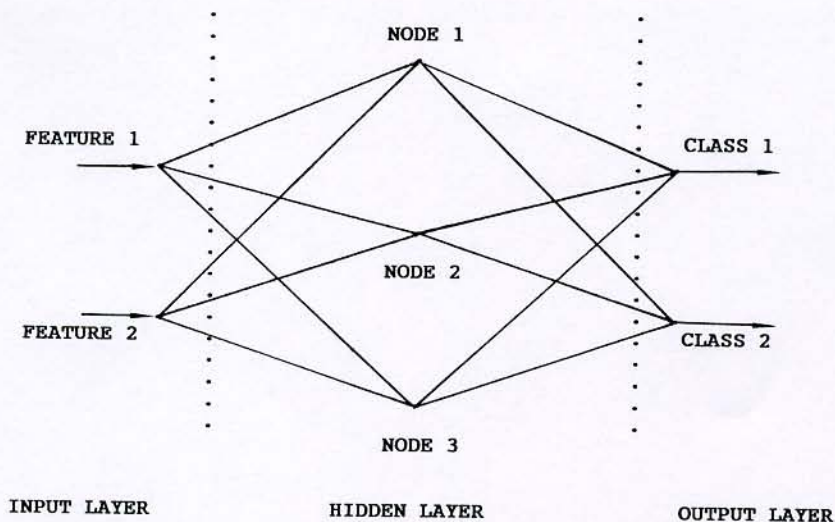


Figure 2. Multilayer perceptron classifier with one hidden layer and three hidden nodes.

and for a hidden layer node by equation (5)

$$d(j) = y(j)(1 - y(j)) \sum_k d(k)w(j, k), \quad (5)$$

where k is associated with all layers nodes to the right of the current node j .

Classification performance was tested by the leave-one-out method [7], and for all possible combinations of the textural features selected in the feature reduction stage. The aim was to determine the optimum combination that achieves the highest classification accuracy with the minimum number of features. Classification performance was also tested for different numbers of hidden nodes and hidden layers, in order to determine the best structural parameters of the MLP classifier. Thus, the final SDEG system includes a section for the computation of the optimum combination of textural features from the lesion's CT density matrix and a section for the classification of the lesion by the MLP classifier into oedema or gliosis.

3. Results

Best textural features, determined in the feature reduction stage ($p < 0.001$), were: variance, skewness, angular second moment, contrast, correlation, entropy, sum entropy, difference variance, and difference entropy. These nine features were used in combinations of 2, 3, 4... , 9 as inputs to the SDEG system, and classification accuracy was evaluated by means of the leave-one-out method. Highest accuracy 89.6% (table 1), was achieved by the contrast-difference entropy feature combination. The SDEG system discriminated correctly 29/35 (82.9%) focal glioses and 40/42 (95.2%) local oedemas. The same classification accuracy (89.6%) was also found for combinations of three, four and five input features; these were combinations of the contrast-difference entropy textural features with either one, two or three of the following: difference variance, sum entropy, angular second moment, correlation, entropy. Employing more than five features the classification accuracy of the system decreased. Figure 3(a) demonstrates the variation of SDEG system performance in relation to the number of textural features.

System accuracy in relation to the number of hidden nodes or hidden layers of the MLP classifier is demonstrated in figure 3(b) and (c), respectively. System performance in relation to the number of passes over the MLP classifier's training set—including all lesion images minus one—is shown in figure 3(d).

Table 1. Two-way truth table demonstrating SDEG system classification of 77 hypodense brain lesions into focal Oedemas and local glioses.

Clinical diagnosis	System classification		Total sums	Percentage accuracy
	Oedemas	Glioses		
Oedemas	40	2	42	95.2
Glioses	6	29	35	82.9
Overall accuracy				89.6

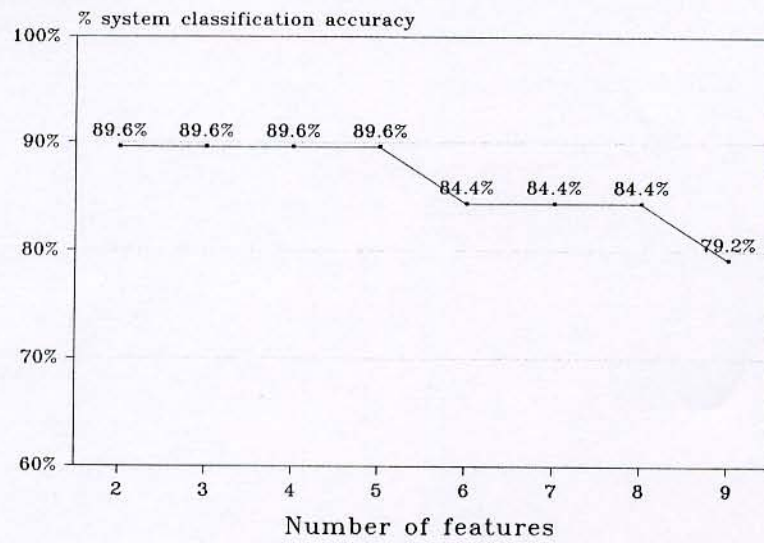
The optimal design parameters of the SDEG system were: contrast-difference entropy input features and one hidden layer—three hidden nodes for the classifier (table 2). Using learning rate $a = 0.2$ and step size $z = 0.7$ in equation (3), maximum accuracy was achieved after 350 passes over the training set of the MLP classifier. Classification of a new lesion by the SDEG system, after input of its CT density matrix, requires < 1 s of computer processing time.

4. Discussion

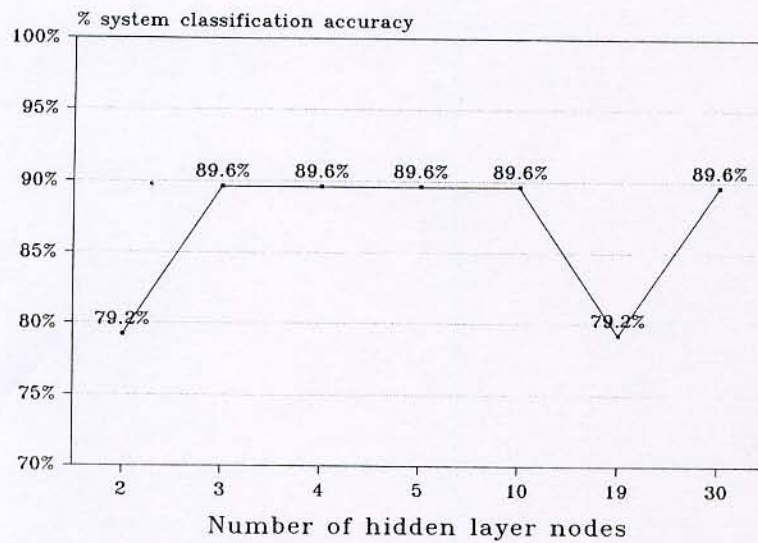
Discrimination between focal oedema and local gliosis is possible by CT when the lesion is extensive; focal oedema is depicted as a space-occupying lesion, while local gliosis is accompanied by signs of cerebral tissue loss and by regional widening of the subarachnoid space. Yet these radiological findings are not clearly evident when the damage is small. On the other hand, the lesion's internal structure depicted on CT usually does not provide diagnostic information, since both focal oedema and local gliosis appear homogeneous and have similar mean attenuation values. By re-scanning the damaged area with thinner CT sections and injecting contrast material intravenously, one may improve the definition of the lesion's margin. However, the disadvantages associated with radiation exposure or iodine contrast media administration in children should be taken into consideration. Here the internal structure of these lesions was examined employing computer image analysis methods and utilizing textural features, which are difficult to perceive visually. Although image analysis methods have been employed in the diagnosis of breast [8, 9], liver [7, 10], and lung [11] lesions, to our knowledge such methods have not been used in the classification of brain damage by CT.

In the initial stage of the SDEG system design, nine features with high ability in discriminating oedemas from glioses were selected. This reduction in feature space dimensionality was important, since it is computationally cumbersome to test system performance with all possible combinations of the 16 initially calculated features. Highest classification accuracy was achieved by a two-feature combination, while system performance did not improve by increasing the number of combined features, probably because of feature intercorrelation. Contrast-difference entropy was the optimum combination giving the highest discriminating power with the minimum number of features. Contrast corresponds to the degree of local variations in the CT density matrix of the lesion, while difference entropy, although it quantifies image structural information, cannot be attributed to a specific textural characteristic [3].

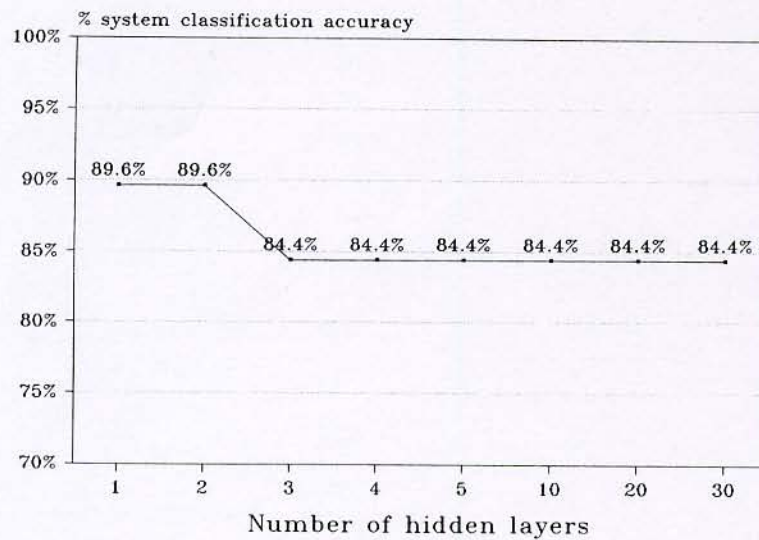
Highest classification accuracy was achieved by one hidden layer and three hidden nodes in the MLP classifier. Using greater number of nodes and/or layers



(a)



(b)



(c)

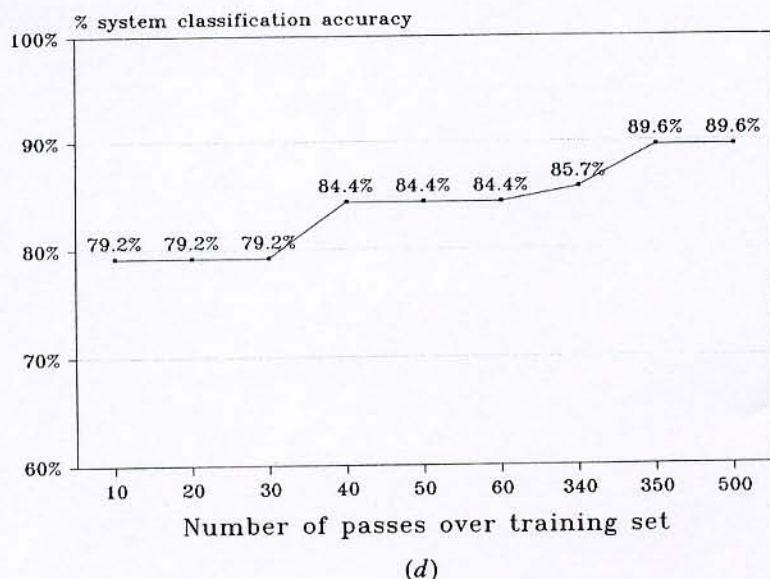


Figure 3. SDEG system performance in relation to the number of (a) textural features (one hidden layer, three hidden layer nodes), (b) hidden nodes (two best features, one hidden layer node), (c) hidden layers (two best features, three hidden layer nodes), and (d) passes over the multilayer perception training set (two best features, three hidden layer nodes).

Table 2. SDEG system design parameters.

Textural features:

$$\text{Contrast} = \sum_{k=0}^{n-1} k^2 \left\{ \sum_{\substack{i=1 \\ k=|i-j|}}^N \sum_{j=1}^N P(i,j) \right\} \quad (1)$$

$$\text{Difference entropy} = - \sum_{i=0}^{N-1} P_{x-y}(i) \log \{P_{x-y}(i)\}, \quad (2)$$

where

N = number of grey levels

$P(i,j)$ = (i,j) th entry of co-occurrence matrix. This corresponds to the mean number of occurrences of i and j grey tones, one pixel apart, in the 0, 45, 90 and 135° directions.

$$P_{x-y}(k) = \sum_{\substack{i=1 \\ k=|i-j|}}^N \sum_{j=1}^N P(i,j), \quad k = 0, 1, 2, \dots, N-1. \quad (3)$$

Multilayer perceptron classifier:

Hidden layers: 1

Hidden layer nodes: 3

Weights between nodes: $w(i,j)$, i is the previous layer node and j is the current layer node.

Input layer – Hidden layer:

$$\begin{aligned} w(1,1) &= 4.929 & w(2,1) &= -1.436 \\ w(1,2) &= 1.887 & w(2,1) &= -5.489 \\ w(1,3) &= -3.339 & w(2,1) &= 2.489 \end{aligned}$$

Hidden layer – Output layer:

$$\begin{aligned} w(1,1) &= 6.060 & w(2,1) &= 7.310 & w(3,1) &= -3.546 \\ w(1,2) &= -6.405 & w(2,2) &= -6.694 & w(3,2) &= 3.462 \end{aligned}$$

the classification accuracy did not improve, while system design complexity increased. The advantage of incorporating more nodes than necessary in a neural network classifier is to give a higher degree of system fault tolerance, in case some hidden nodes fail to function [5].

In clinical practice, radiological discrimination between focal oedema and local gliosis is based on the patient's history and on CT signs concerning the lesion's effect on neighbouring brain parenchyma. Here discrimination is based on information extracted from the lesion's internal structure that cannot be obtained by visual inspection. Thus, the proposed SDEG system offers additional information, which may be valuable especially in cases of small brain lesions that cause minimal effect to the surrounding parenchyma.

5. Conclusions

The application of image analysis methods to the CT image matrix of hypodense cerebral lesions reveals textural information not evident by visual inspection. Two textural features, extracted from the co-occurrence matrix of the lesion's CT image, and an efficient neural network classifier, forms a software system that automatically distinguishes focal oedemas from local glioses with good accuracy. This information can be used by the physician, together with other radiological criteria, in the differential diagnosis between brain focal oedemas and local glioses. The proposed system may be particularly useful in small cerebral lesions, where distinction between these two types of brain damage is radiologically difficult.

Acknowledgement

We gratefully acknowledge Mr S. Goufopoulos and Mr I. Dalezios for their assistance in the collection and preliminary processing of the material of this work.

References

1. BARKOVICH, A. J. (1990) *Pediatric Neuroimaging* (New York: Raven), pp. 205–226.
2. LEE, S. H., RAO, K. C. V. G. and ZIMMERMAN, R. A. (1992) *Cranial MRI and CT* (New York: McGraw Hill), pp. 701–733.
3. HARALICK, R. M., SHANMUGAM, K. and DINSTENK, I. (1973) Textural features for image classification. *IEEE Transactions on Systems, Man, and Cybernetics*, **SMC-3** (6), 610.
4. HARALICK, R. M. (1979) Statistical and structural approaches to texture. *Proceedings of the IEEE*, **67** (5), 786.
5. KHOTANZAD, A. and LU, J. H. (1990) Classification of invariant image representations using a neural network. *IEEE Transactions on Acoustics, Speech, and Signal Processing*, **38** (6), 1028.
6. KELLY, M. F., PARKER, P. A. and SCOTT, R. N. (1990) The application of neuron networks to myoelectric signal analysis: a preliminary study. *IEEE Transactions on Biomedical Engineering*, **37** (3), 221.
7. RAETH, U., SCHLAPS, D., LIMBERG, B., ZUNA, I., LORENZ, A., VAN, KAIK, G., LORENZ, W. J. and KOMMERELL, B. (1985) Diagnostic accuracy of computerized B-scan texture analysis and conventional ultrasonography in diffuse parenchymal and malignant liver disease. *Journal of Clinical Ultrasound*, **13** 87.
8. RICHTER, J. H. and CLARIDGE, E. (1991) Extraction of quantitative blur measures for circumscribed lesions in mammograms. *Medical Informatics*, **16** (2), 229.
9. FINETTE, S., BLEIER, A. R., SWINDELL, W. and HABER, K. (1983) Breast classification using diagnostic ultrasound and pattern recognition techniques: II. Experimental results. *Ultrasonic Imaging*, **5**, 71.
10. LERSKI, R. A., SMITH, M. J., MORLEY, P., BARNETT, E., MILLS, P. R., WATKINSON, G. and MACSWEEN, R. N. (1981) Discriminant analysis of ultrasonic texture data in diffuse alcoholic liver disease. *Ultrasonic Imaging*, **3**, 164.
11. CAVOURAS, D., PRASSOPOULOS, P. and PANTELIDIS, N. (1992) Image analysis methods for solitary pulmonary nodule characterization by computed tomography. *European Journal of Radiology*, **14**, 169.